Electronic defects in the halide antiperovskite semiconductor Hg_{3}Se_{2}I_{2}

Joon-Il Kim, John A. Peters, Yihui He, Zhifu Liu, Sanjib Das, Oleg Y. Kontsevoi, Mercouri G. Kanatzidis, and Bruce W. Wessels

Electronic Defects in the Halide Anti-perovskite $Hg_3Se_2I_2$ Semiconductor

Joon-Il Kim[1], John A. Peters[1,3], Yihui He[2], Zhifu Liu[1], Sanjib Das[1], Oleg Y. Kontsevoi[4], Mercouri G. Kanatzidis[1,2], and Bruce W. Wessels[1]

[1]*Department of Materials Science and Engineering, Northwestern University, Evanston, IL, USA*
[2]*Department of Chemistry, Northwestern University, Evanston, IL, USA*
[3]*Department of Chemistry and Physics, Chicago State University, Chicago, IL, USA*
[4]*Department of Physics and Astronomy, Northwestern University, Evanston, IL, USA*

Abstract

Halide perovskites have emerged as a potential photoconducting material for photovoltaics and hard radiation detection. We investigate the nature of charge transport in the semi-insulating chalcohalide $Hg_3Se_2I_2$ compound using the temperature dependence of dark current, thermally stimulated current (TSC) spectroscopy, and photoconductivity measurements as well as first-principles density functional theory (DFT) calculations. Dark conductivity measurements and TSC spectroscopy indicate the presence of multiple shallow and deep level traps that have relatively low concentrations of the order of $10^{13} – 10^{15}$ cm^{-3} and capture cross sections of $\sim 10^{-16}$ cm^2. A distinct persistent photoconductivity (PPC) is observed at both low temperatures (< 170 K) and high temperatures (> 230 K), with major implications for room temperature compound semiconductor radiation detection. From preliminary DFT calculations, the origin of the traps is attributed to intrinsic vacancy defects (V_{Hg}, V_{Se}, and V_I) and interstitials (Se_{int}) or other extrinsic impurities. The results point the way for future improvements in crystal quality and detector performance.

Keywords: kinetics, chalcohalide, deep level, radiation detection, persistent photoconductivity, thermally stimulated current.

Introduction

Hard radiation detection at room temperature is now a universal concern. There are huge demands for X- and γ-ray detectors that operate at room temperature in the science of astronomy and applications of industrial and medical imaging, as well as in nuclear safeguard and national security. The search for alternatives to CdZnTe, the currently preferred semiconductor, as a room-temperature hard radiation detector material has intensified in recent years due to its high cost and seemingly unavoidable growth issues, particularly microstructural defects [1-3]. Consequently, there has been a concerted effort to develop new low-cost semiconductor materials with much improved detection properties. Recently perovskite structure compound semiconductors have shown considerable promise for these applications. Using the concept of lattice hybridization, the anti-perovskite structure ternary compound Hg-based chalcohalides $Hg_3Q_2X_2$ (Q = S, Se, Te; X = I, Cl, Br) have been identified and recently proven to be very promising and cost-effective for X-ray and γ-ray detection at room temperature [4-7]. In the family of $Hg_3Q_2X_2$ compounds the diverse ordering of the Hg vacancies in the crystal structure can be described universally as anti-perovskite based. This ordering varies depending on Q and X and yields a rich family of crystal structures ranging from zero-dimensional to three-dimensional, with a dramatic effect on the properties of each compound [7]. In addition to their excellent stability, these compounds have high specific densities ranging from 6.83 g/cm^3 to 7.78 g/cm^3 and energy band gaps of 2.0 eV $< E_g <$ 2.6 eV [4]. Their intrinsic electrical resistivity is on the order of $10^{11} - 10^{12}$ Ω·cm [7]. Recently, large and high-quality single crystals of these compounds have been grown by the Bridgman and vapor transport methods with each material showing excellent photo sensitivity under energetic photons [7]. Detectors made from thin $Hg_3Q_2X_2$ crystals show reasonable response under a series of radiation sources, including Ag X-

ray, [241]Am, and [57]Co radiation. The carrier mobility-lifetime ($\mu\tau$) product for $Hg_3Q_2X_2$ detectors, a figure of merit for charge transport, is on the order of 10^{-4} to 10^{-6} cm^2/V [7]. On the basis of the photoconductivity and hard radiation detection measurements, these $Hg_3Q_2X_2$ crystals could offer a low-cost alternative for room temperature radiation detectors.

Among the family of Hg chalcohalide compounds, $Hg_3Se_2I_2$ crystals show the most promise for room-temperature radiation detection, with an electron mobility estimated as 104 ± 12 cm^2/Vs and a lifetime of 100 ns leading to a mobility-lifetime ($\mu\tau$) product of 1.0×10^{-5} cm^2/V [7]. Some of the advantages of this compound include an optical bandgap of 2.15 eV (*indirect*), a high specific density of 7.38 g/cm^3, and a small electron effective mass of $m_e{}^* \sim 0.2m_0$ [7]. $Hg_3Se_2I_2$ detectors have achieved spectroscopic resolution for both [241]Am α-particles (5.49 MeV) and [241]Am γ-rays (59.5 keV), with full widths at half-maximum (FWHM, in percentage) of 19% and 50%, respectively [7]. Further improvements in detector response are expected to result from increases in carrier lifetime. The question then arises as to what limits the lifetime. Is it carrier scattering, Shockley-Read Hall (SRH) recombination, or carrier trapping? In this work, we report on a detailed investigation of charge transport in semi-insulating $Hg_3Se_2I_2$ crystals to determine the role defects play in limiting its detector performance and photoconductive response. The charge carrier kinetics were analyzed using the temperature dependence of dark current, thermally stimulated current (TSC) spectroscopy, and photoconductivity measurements.

Experimental details

Semi-insulating $Hg_3Se_2I_2$ single crystals were grown using a chemical vapor transport (CVT) method reported elsewhere [7]. For the growth of compound $Hg_3Se_2I_2$ via vapor transport, the challenges include the management of the high vapor pressures of the Hg, Se and I components, and the control of zone temperatures to accommodate each partial pressure. Efforts

to accommodate each partial pressure were taken, and thus succeeded in growing single crystal samples with appreciable dimensions. In addition, the vapor transport process also has a beneficial effect of self-purification, which presumably leads to better performance [7].

According to its phase diagram, the compound $Hg_3Se_2I_2$ melts incongruently at 420 °C [8]. In order to grow such an incongruently compound from its melt, we tested different ratios of the starting materials (HgI2:HgSe), from stoichiometric to heavily HgI_2 rich conditions, but found that no one gave rise to large single crystals [7]. It should be noted that with heavily HgI_2 rich conditions during cooling, HgI_2 suffers a destructive phase-transition around 127 °C, which likely destroys the ternary crystal already grown. The thickness of the grown $Hg_3Se_2I_2$ crystals is in the range of 0.2 − 0.4 mm. For different samples, the temperature distributions within the cold- and hot-zones during vapor growth was varied in the aim to find those with better yield and improved transport properties. Specifically, sample YH1157 has better yield comparing to that of sample YH1129 due to the former's closer to optimal thermal distribution of the temperature field. The thicknesses are around 0.2 mm. For electrical measurements, a 50-nm-thick layer of Au was deposited on both sides of the sample by electron beam evaporation to form electrodes. To determine the sample resistivity, 2-terminal $I-V$ characteristics were measured by applying a low bias voltage from - 10 V to 10 V. For temperature dependence of the dark and photocurrent and photo-excitation measurements, either positive or negative bias was applied to the electrode by an Agilent E3610A DC power supply. The current was measured by using a Keithley 2636A source meter. A CW semiconductor diode laser with emission at 405 nm was used for photoexcitation. To conduct thermally stimulated current (TSC) spectroscopy measurement, the sample was mounted in a cryostat and cooled down in the dark to 80 K. Subsequently at 80 K, the sample was photo-excited (400 mW/cm^2 intensity of a 405-nm laser) for approximately 13

min to place the sample in a nonequilibrium state. About 10 minutes after the laser was turned

off, the sample was then heated up from 80 K to 200 K at a constant rate of 0.13 K/s and from

200K to 320 K at a rate of 0.08 K/s.

Results and Discussion

Temperature dependence of dark current (I$_D$-T)

The temperature dependence of the dark current was measured to determine the dominant

conduction mechanisms in semi-insulating Hg$_3$Se$_2$I$_2$ detector devices. The dark current I_D is

described by a summation of dark current components with different activation energies:

$$I_D = \sum_i I_{0i} e^{-E_{ai}/kT} , \tag{1}$$

where I_{0i} is a prefactor for the ith component, E_{a_i} is an activation energy, and k is the Boltzmann

constant. Figure 1 shows an exponential increase of dark current with increasing temperature

from 80 K to 320 K under a negative bias voltage of -5 V. As shown in Fig. 1, there are two

distinct characteristic slopes in the temperature dependence of the dark current. The activation

energies are extracted from the Arrhenius plots of the dark current. The activation energies at

low and high temperature (inset of Fig. 1) are 0.05 eV and 0.70 eV for sample YH1129, which is

attributed to Shockley-Hall-Read (SRH) charge transport involving shallow and deep level

defects, respectively. The activation energies for the measured samples are listed in Table 1. As

can be seen, activation energies in the range $0.7 - 1.15$ eV are observed at high temperature (275

K $< T <$ 325 K), which is tentatively attributed to ionization of deep electronic states. The

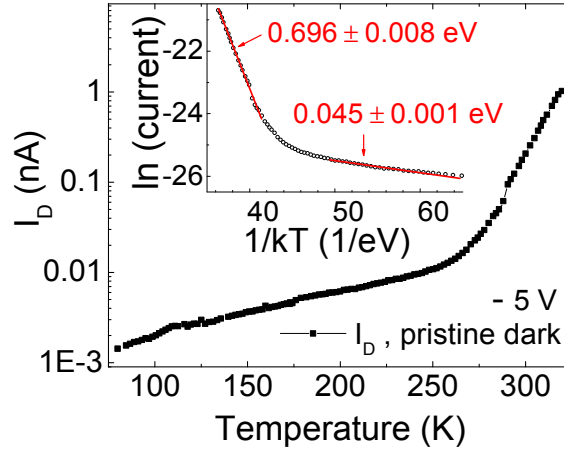ionization energy of 0.05 ± 0.01 eV at low temperature is attributed to shallow electronic states.

FIG. 1. Temperature dependence of the pure dark current for $Hg_3Se_2I_2$. Inset: Arrhenius plot of the pure dark current of sample YH1129. The bias voltage is -5 V from the top electrode to the bottom electrode.

Table 1. The calculated activation energies and the resistivity under negative and positive bias voltages for a series of $Hg_3Se_2I_2$ samples.

Sample ID	Reverse bias (-5 V)		Forward bias (+5 V)		$\rho_{(-)}$	$\rho_{(+)}$
	$E_{a1,n}$ (eV)	$E_{a2,n}$ (eV)	$E_{a1,p}$ (eV)	$E_{a2,p}$ (eV)	$(\times 10^{10}\,\Omega cm)$	$(\times 10^{10}\,\Omega cm)$
YH1129	0.70 ± 0.01	0.05 ± 0.001	0.71 ± 0.01	0.04 ± 0.001	4.3 ± 1.9	3.5 ± 1.7
YH1157A	1.15 ± 0.02	0.04 ± 0.01	0.82 ± 0.01	0.02 ± 0.02	16 ± 8	20 ± 11
YH1157D1	0.94 ± 0.01	0.02 ± 0.004	0.91 ± 0.01	0.07 ± 0.02	70 ± 41	61 ± 9
YH1157D2	0.70 ± 0.01	0.04 ± 0.01	0.83 ± 0.02	0.05 ± 0.01	24 ± 4	92 ± 33

Thermally stimulated current spectroscopy

To investigate the nature of the defects involved in charge transport, thermally stimulated current spectroscopy (TSC) measurements were conducted over the temperature range of 80 – 320 K. This technique has been widely employed to determine deep level defect energies in highly resistive semiconductor materials [9],[10]. The thermally stimulated current, resulting

from a return to equilibrium, was measured as a function of temperature. As shown in Fig. 2, the

TSC results clearly revealed peaks over the temperature range from 80 K to 320 K.
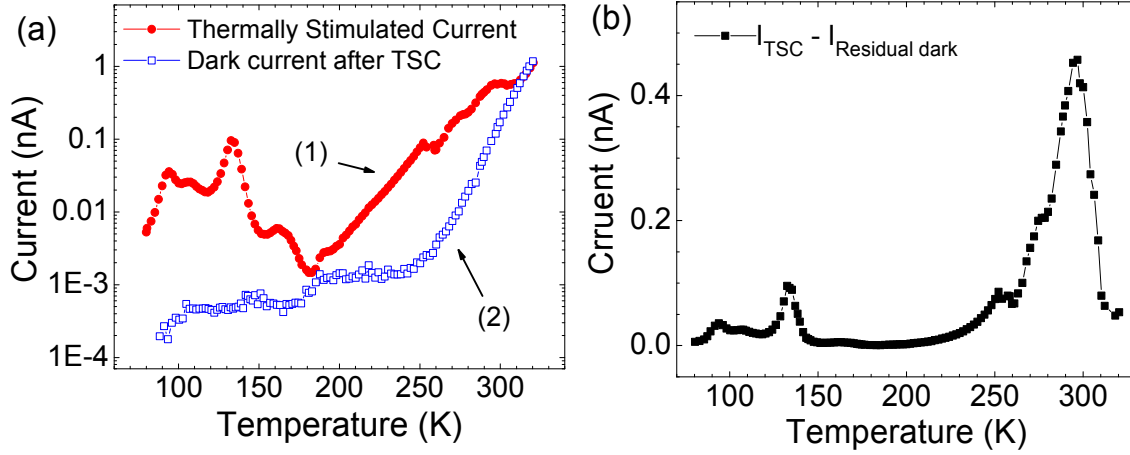

FIG. 2. (a) Thermally stimulated current spectrum for sample YH1157D2 (1) and residual dark current after TSC measurement (2). (b) Thermally stimulated spectrum after subtracting curve (2) from curve (1) in (a).

A careful analysis of the TSC spectrum in Fig. 2(b) reveals at least four peaks below 180

K and three peaks observed above 250 K, as shown in Fig. 3. The maxima T_m of the peaks gives

an approximate trap energy. According to Bube [9], the energy level of the trap, E_t, is given by:

$$E_t = kT_m \ln \frac{NSv_{th}kT_m^2}{\beta E_t}, \tag{2}$$

where T_m is the TSC peak temperature, N is the effective density of states, S is the capture cross section,

v_{th} is the thermal velocity of carriers, k is the Boltzmann constant, and β is the heating rate. Eq. (2) can

be rearranged with the temperature dependence of $N \sim T^{3/2}$ and $v_{th} \sim T^{1/2}$ as [9],[11]

$$E_t = kT_m \left(\ln \frac{T_m^4}{\beta} + \ln \frac{2 \times 10^{16} S_n}{E_t} \right), \tag{3}$$

for electron traps. By using the quasi-equilibrium approach of Bube and Fang [9],[12], the trap

depth, E_t, can be approximated using,

$$E_t = kT_m \ln\left(\frac{T_m^4}{\beta}\right). \tag{4}$$

In general, the approximation represented by Eq. (4) is only useful to estimate trap depths due to the uncertainty in the magnitude of the capture cross section. As seen in Fig. 3(a) and 3(b), a total of nine traps are observed, labeled $T_1 - T_9$. These trapping centers are tentatively considered as electron traps, since the peaks only appear if illumination occurs through the negatively biased contact. The trap concentration, N_{T_i}, can be determined approximately from [12,13]

$$N_{T_i} = \frac{Q_{T_i}}{2\,\mu\tau e A E} \tag{5}$$

where the charge Q_{T_i} is the temporal integration of each fitted TSC peak spectrum defined by $Q_{T_i} = \int I_{TSC}^i dt = \frac{1}{\beta}\int_{T_0}^{T} I_{TSC}^i dT$, μ is the carrier mobility, τ is the carrier lifetime, e is the electron charge, A is the area of electrode, and E is the applied electric field. The capture cross section, S_i, is given by [14]:

$$S_i = \frac{\beta E_t}{kT_m^2 N v_{th}}\exp(E_t/kT_m). \tag{6}$$

Using Eqs. (4), (5), and (6), the trap depths, trap densities, and capture cross sections for the observed traps were calculated and are listed in Table 2. It is worth noting that the traps observed in $Hg_3Se_2I_2$ have relatively low concentrations ranging from 4.0×10^{13} cm^{-3} to 5.3×10^{15} cm^{-3}, indicating reasonably good quality crystals. By comparison, the trap concentrations for Cadmium Zinc Telluride (CZT) is also in the range of 10^{13} cm^{-3} to 10^{15} cm^{-3} [15,16]. However, the capture cross sections of 10^{-16} cm^2 for $Hg_3Se_2I_2$ are two to five orders of magnitude higher than that of CZT crystals, indicating these are neutral traps. The small capture cross sections in CZT are

attributed to the effective screening of defects which contributes to their excellent carrier transport [15,16].
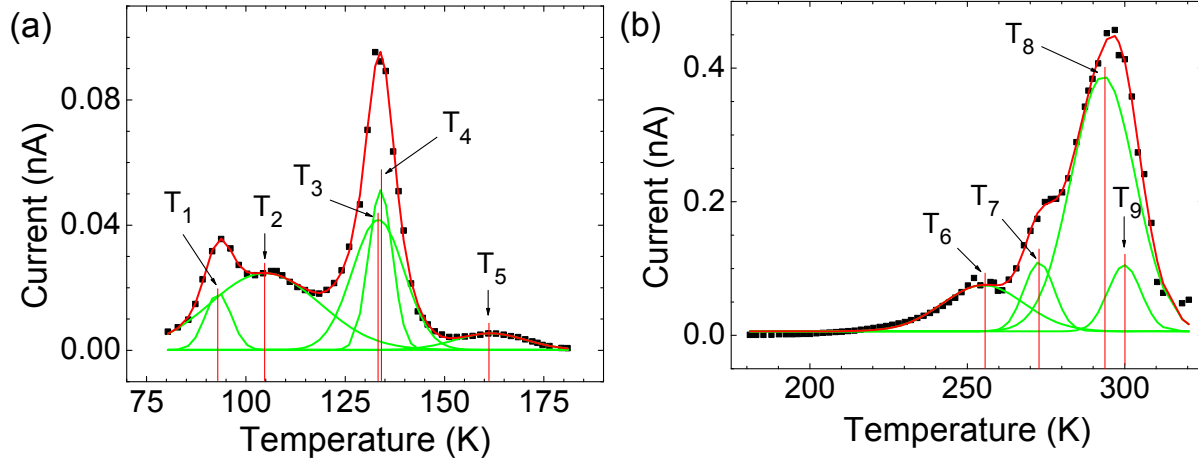

FIG. 3. Deconvoluted peaks of thermally stimulated spectrum after subtracting the dark current in the temperature range of (a) 80 K – 180 K (b) 180 K – 320 K.

Table 2. The peak temperatures, extracted trap energies, their densities, and capture cross sections for the TSC peaks (Sample YH1157D2).

	80 K – 180 K				180 K – 320 K		
T_m (K)	$E_{t,m}$ (eV)	N_{T_m} ($\times 10^{14}$cm^{-3})	S_i ($\times 10^{-16}$cm^2)	T_m(K)	$E_{t,m}$(eV)	N_{T_m} ($\times 10^{14}$cm^{-3})	S_i ($\times 10^{-16}$cm^2)
T_1 93	0.16	0.5	1.2	T_6 255	0.54	12	4.1
T_2 105	0.19	2.9	1.4	T_7 273	0.59	6.9	4.4
T_3 133	0.25	2.3	1.9	T_8 293	0.64	53	4.8
T_4 134	0.25	1.3	1.9	T_9 300	0.65	7.2	4.9
T_5 162	0.31	0.4	2.4				

Calculations using density functional theory

Regarding the identity and nature of the defects obtained from the TSC and dark conductivity measurements, preliminary first principles density functional theory (DFT) calculations indicate that disorder in $Hg_3Se_2I_2$ arises from intrinsic point defects including vacancies, antisite disorder, and interstitials. Figure 4 shows the crystal structure of $Hg_3Se_2I_2$

represented by a ball and stick model. Hg and I atoms are each present in three different lattice sites. There are seven types of vacancy defects (3 V_{Hg}, 1 V_{Se}, and 3 V_I), fourteen types of antisite defects (3 Se_{Hg}, 3 I_{Hg}, 1 Hg_{Se}, 1 I_{Se}, 3 Hg_I, and Se_I), and twenty-one possible types of interstitial defects (7 Hg_{int}, 7 Se_{int}, and 7 I_{int}). From the calculations of defect formation energies, V_{Hg}, V_{Se}, and V_I are the most dominant defects, whereas Se_{int} defects become dominant in Se-rich growth conditions. The ionization energies for these native defects indicate that the interstitial defect Se_{int} is a localized level located close the middle of the gap. In a neutral state, this defect is a deep donor. Thus, by comparing the activation energies from dark conductivity (Table 1) and TSC (Table 2) to those from DFT calculations, the defect levels in the range $0.54 - 1.15$ eV are presumably due to the selenium interstitials Se_{int} or to other extrinsic impurities that were not considered in the DFT calculations. The defect levels in the range $0.16 - 0.31$ eV are presumably due to vacancy defects (V_{Hg}, V_{Se}, and V_I). In order to reduce carrier trapping effects it is desirable to have low concentrations of the deep centers (Se_{int}) in $Hg_3Se_2I_2$ crystals.

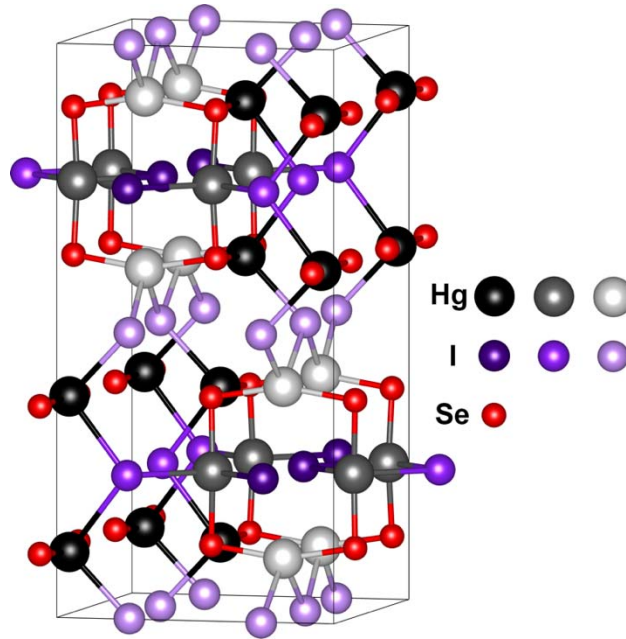FIG. 4. The crystal structure of $Hg_3Se_2I_2$. Black, gray and light gray balls correspond to Hg atoms at three different lattice sites. Dark purple, purple and light purple balls correspond to three types of I atoms. Se atoms are represented by the red balls.

Photoconductivity and persistent photoconductivity (PPC)

To determine which mechanism best describes the origin of the photoconductivity in $Hg_3Se_2I_2$, temperature dependence of photocurrent was measured under a bias voltage of -5 V in the temperature range $80 - 320$ K (Fig. 5). The photocurrent was measured with 2 K increment steps and a 15 s delay time to stabilize the current at each temperature. The magnitude of the photoconductivity depends on the mobility-lifetime product. In general, photoconductivity $\Delta\sigma_{ph}(T)$ can be written as a function of temperature [17] given by the equation:

$$\Delta\sigma_{ph}(T) = G(T)[e\tau_e(T)\mu_e(T) + h\tau_h(T)\mu_h(T)], \qquad (7)$$

where $G(T)$ is the generation rate of electron-hole pairs, τ_e and τ_h are the electron and hole lifetime respectively, and μ_e and μ_h are the carrier mobility of electrons and holes. The generation rate can be assumed to be constant over the entire temperature range when above-gap light is used, and the sample thickness is much greater than the expected penetration depth of the light. Since the $Hg_3Se_2I_2$ samples are highly resistive and contain a number of deep level defect states, the lifetime of carriers is dominated by the Shockley-Read-Hall (SRH) recombination [17]. As shown in Fig. 5, below 250 K the photoconductivity is moderately enhanced with decreasing temperature. This behavior suggests that impurity scattering due to defects is dominant at low temperatures (80 K $< T < 250$ K), thereby suppressing the mobility and consequently the photoconductivity according to Eq. (7).
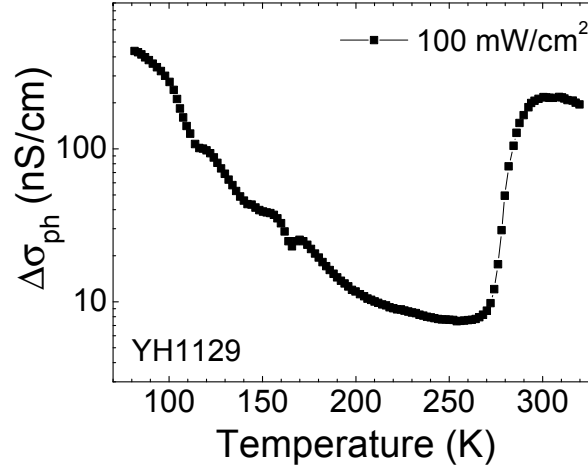
FIG. 5. Temperature dependence of photoconductivity under -5 V for sample YH1129. 100 mW/cm^2 intensity of 405 nm laser was used for photoexcitation.

Photosensitivity (/) of the Hg$_3$Se$_2$I$_2$ samples was also determined by illuminating the crystal with a 405-nm diode laser excitation. Here $\Delta\sigma$ is the change in the conductivity upon illumination and σ is the conductivity in the dark. / values of ~1^4 and 10 were measured at low and room temperatures, respectively. After photoexcitation was terminated, however, a high residual leakage current, a persistent photocurrent (PPC), was observed. This can be seen in Fig. 6(a) that shows the variation of current with time before, during, and after photoexcitation. The PPC persisted for 10 - 24 hours depending on sample and illumination conditions. The time decay of the PPC after laser excitation was terminated is shown in the inset of Fig. 6(a). The excitation intensity of the laser was 100 mW/cm^2. The decay curve can be described by the well-known stretched exponential function for complex relaxation kinetics, given by [18-22]:

$$I_{PPC}(t) \; = \; I_{PPC}(0) \exp\left[-(t/\tau)^{\beta}\right], \tag{8}$$

where $I_{PPC}(0)$ is the current at the instant when the light illumination is terminated, τ is the PPC decay time constant, and β is a characteristic exponent. When $\beta = 1$, Eq. (8) describes a first order decay process, but when β is less than 1, the decay involves a distribution of time decay

constants. A larger β value in the range of $0 < \beta < 1$ indicates a narrower distribution of time

decay constants while a smaller β value indicates a wider distribution of time decay constants.

The values of τ and β determined using the stretched exponential fitting are 46.5 ± 3.8 min and

0.65 ± 0.05, respectively at 295 K. The β value of 0.65 ± 0.05 indicates rather narrow

distribution of time decay constants. Hence, we ascribe the PPC effect to multiple transitions

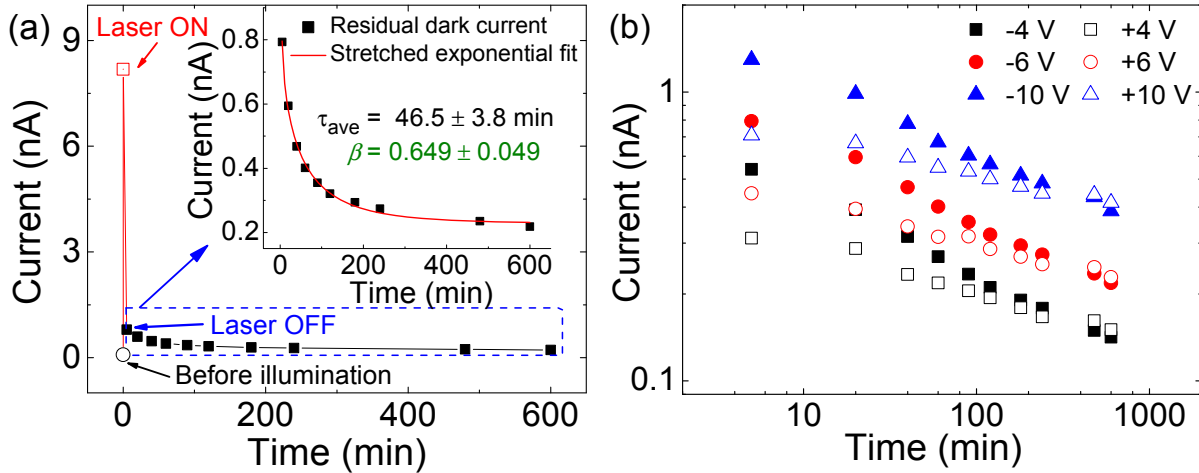involving defect states within the gap of the material as described by Luo et al. [23].

FIG. 6. (a) Variation of current with time for sample YH1129 at room temperature before (open circle), during (open square), and after (solid squares) laser excitation. Inset: Stretched exponential function fitting of the PPC decay curve at room temperature. (b) Time evolution of the dark current at room temperature under various bias voltages after the illumination was terminated.

To compare the dark conductivity and PPC effect before and after the sample

illumination, the temperature dependence of the dark current and photocurrent was measured in

the following sequence. First, the sample was cooled down to 80 K in the dark and the pristine

dark current was measured while the sample was warmed up to 320 K at a rate of 0.13 K/sec

(solid blue squares in Fig. 7). The sample was then cooled down again to 80 K, and the dark and

photocurrent were alternatively measured during the warm up to 320 K (solid black circles for

OFF state and open red circles for ON state in Fig. 7). The laser (400 mW/cm^2) was ON for 4 s

to measure the photocurrent at each temperature. Finally, to investigate the duration of the PPC

the dark current was again measured with increasing temperature from 80 K to 320 K at a rate of

0.13 K/sec (open purple triangles in Fig. 7). As shown in Fig. 7, all the dark current curves

(including the current with OFF state laser power) differ from one another, which indicates that

there are two distinct PPC effects – one below ~170 K and another above ~230 K. Interestingly,

while the PPC in the low temperature region is quenched at ~170 K during the warm up process,

the observed PPC above 230 K (open purple triangles in the Fig. 7) remains until 320 K. This

difference clearly shows there are different origins for the low temperature PPC and the room

temperature PPC. Upon correlating our charge transport measurements to the DFT calculations,

we tentatively attribute the PPC observed in Hg$_3$Se$_2$I$_2$ crystals at low temperature to these

intrinsic vacancy defects (V$_{Hg}$, V$_{Se}$, and V$_I$) while the PPC observed at high temperature is most

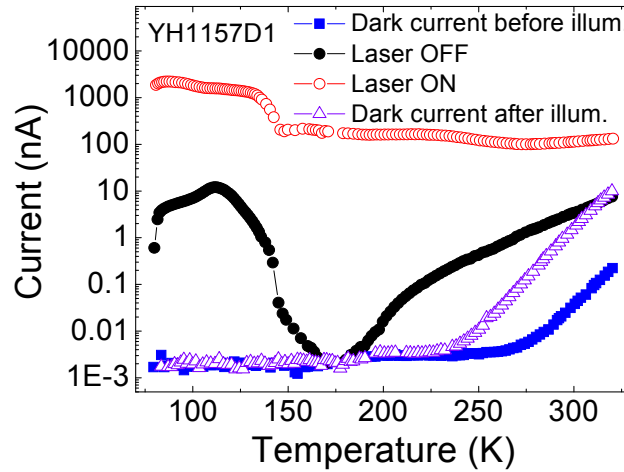likely due to intrinsic selenium interstitial point defects and/or other extrinsic impurities.

FIG. 7. Temperature dependence of dark currents (before, during, and after illumination) and photocurrent under -5 V for sample YH1157D1 sample. 400 mW/cm^2 intensity of 405 nm laser was applied.

Figure 8 shows the configuration-coordinate model that describes the PPC effect. Upon photoexcitation, electrons are excited from the valence band (E_V) into the conduction band (E_C) leading to photoconductivity. Thermal quenching of the photoconductivity results when electrons are captured by the defect level, D [24]. Capture requires overcoming the energy barrier labeled, E_B. In the case where neutral defects are charged by trapping of photoexcited carriers (dashed curve in Fig. 8), the barrier, E_B, will be modified due to coulombic interaction. The barrier height, E_B, depends on the magnitude of the lattice relaxation the defect undergoes upon electron capture. The barrier prevents the photoexcited electrons in the conduction band from being captured by the defect state. When the electrons in the conduction band have sufficient thermal energy to overcome the barrier E_B, the PPC will be quenched. Subsequently, the electrons captured by the defect can either recombine non-radiatively with holes in the valence band or ionize to the conduction band.
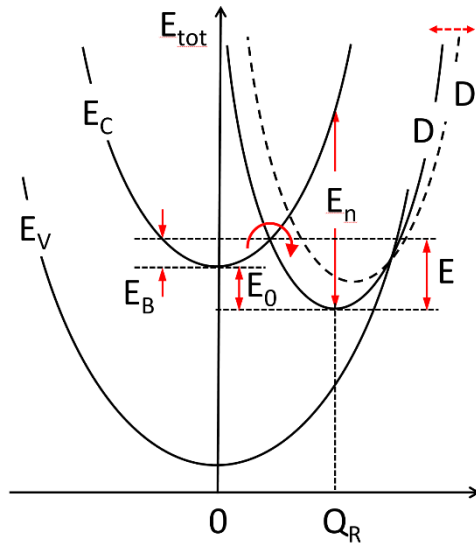

FIG. 8. Schematic configuration-coordinate diagram for PPC. E_C and E_V are the conduction and valence band, respectively. D and D' are the ground and excited states of the defect. The energy E_n is the photoionization threshold for the defect. E_B is the capture barrier height, E_0 is the thermal binding energy of the state, and E is the thermal height of the thermal barrier for electron emission from the deep center to the conduction band [25].

Summary and Conclusions

In summary, the charge transport properties of defect anti-perovskite $Hg_3Se_2I_2$ single crystals were investigated over the temperature range of 80 – 320 K. The as-grown crystals exhibit high intrinsic electrical resistivity on the order of 10^{11} $\Omega \cdot cm$. We observed an exponential dependence on temperature of the dark current with activation energies in the range of 0.02 – 0.07 eV and 0.70 – 1.15 eV in the low and high temperature regimes, respectively. The single crystals showed a colossal photosensitivity ($\Delta\sigma/$. of $\sim10^4$ below 170 K.

TSC spectroscopy was used to characterize the traps in the $Hg_3Se_2I_2$ compound. At least nine trapping centers were observed in the temperature range from 93 to 300 K. All the discrete traps measured, with energy levels of 0.16 – 0.65 eV, have relatively low concentrations of the order of 10^{13} – 10^{15} cm^{-3} and capture cross sections of $\sim10^{-16}$ cm^2. Based on first principles density functional theory, traps T_1 – T_5 (0.16 – 0.31 eV) were attributed to vacancy defects (V_{Hg}, V_{Se}, and V_I) while traps T_6 – T_9 (0.54 – 0.65 eV) were attributed to Se interstitials and/or other extrinsic impurities.

Persistent photoconductivity was observed in $Hg_3Se_2I_2$ at both low temperature and room temperature. The PPC was described by a configuration coordinate diagram involving electron transitions between the conduction and a deep donor level. Likewise, the low temperature PPC was attributed to intrinsic vacancy defects (V_{Hg}, V_{Se}, and V_I) while the high temperature PPC was due to intrinsic Se interstitials and/or other extrinsic impurities, based on preliminary DFT calculations. By analyzing the room temperature PPC excitation and decay kinetics using a stretched exponential function in time, a decay time constant of 47 min was obtained with a characteristic exponent, β, value of 0.65 indicating a narrow distribution of traps energies.

Notwithstanding the presence of native defects/impurities, the potential of $Hg_3Se_2I_2$ as a hard radiation detection material is promising. Further improvements remain to be made in the vapor growth procedure of these compounds through purification of the starting materials and precise control over the crystal stoichiometry. This should lead to larger $\mu\tau$ products and high efficiency detectors that are highly sensitive to X-rays and γ-rays. Future efforts will focus on native defect control and continuing improvement of $Hg_3Se_2I_2$ as a room temperature radiation detector.

Author information

*E-mail: b-wessels@northwestern.edu

References

[1]   M. Amman, J. S. Lee, and P. N. Luke, Journal of Applied Physics **92**, 3198 (2002).

[2]   G. A. Carini, A. E. Bolotnikov, G. S. Camarda, G. W. Wright, R. B. James, and L. Li, Applied Physics Letters **88**, 143515 (2006).

[3]   G. Koley, J. Liu, and K. C. Mandal, Applied Physics Letters **90**, 102121 (2007).

[4]   C. D. Malliakas, A. C. Wibowo, Z. Liu, J. A. Peters, M. Sebastian, H. Jin, D.-Y. Chung, A. J. Freeman, B. W. Wessels, M. G. Kanatzidis, Proc. of SPIE **8507**, 85070F (2012).

[5]   A. C. Wibowo, C. D. Malliakas, H. Li, C. C. Stoumpos, D. Y. Chung, B. W. Wessels, A. J. Freeman, and M. G. Kanatzidis, Crystal Growth & Design **16**, 2678 (2016).

[6]   H. Li, F. Meng, C. D. Malliakas, Z. F. Liu, D. Y. Chung, B. Wessels, and M. G. Kanatzidis, Crystal Growth & Design **16**, 6446 (2016).

[7]   Y. He, O. Y. Kontsevoi, C. C. Stoumpos, G. G. Trimarchi, S. M. Islam, Z. Liu, S. S. Kostina, S. Das, J.-I. Kim, W. Lin, B. W. Wessels, and M. G. Kanatzidis, Journal of the American Chemical Society **139**, 7939 (2017).

[8]   J. Beck and S. Hedderich, Journal of Solid State Chemistry **151**, 73 (2000).

[9]   R. H. Bube, Photoconductivity in Solids. John Wiley & Sons, Inc. (1960).

[10]   A. G. Milnes, *Deep impurities in semiconductors* (Wiley, New York, 1973), xviii, 526 p.

[11]   Z. Q. Fang, S. Lei, T. E. Schlesinger, and A. G. Milnes, Mater. Sci. Eng. B-Solid State Mater. Adv. Technol. **5**, 397 (1990).

[12]   R. H. Nan, W. Q. Jie, G. Q. Zha, T. Wang, Y. D. Xu, and W. H. Liu, Journal of Physics D-Applied Physics **43**, 5, 345104 (2010).

[13]   M. Plodinec, A. Santic, J. Zavasnik, M. Ceh, and A. Gajovic, Applied Physics Letters **105**, 5, 152101 (2014).

[14]   E. M. Zobov, A. Y. Mollaev, L. A. Saipulaeva, A. G. Alibekov, and N. V. Melnikova, Phys. Solid State **58**, 2457 (2016).

[15]   R. O. Pak, K. V. Nguyen, C. Oner, M. A. Mannan, and K. C. Mandal, Proc. SPIE 9593, Hard X-Ray, Gamma-Ray, and Neutron Detector Physics XVII, 95931J (2015).

[16]   R. Gul, A. Bolotnikov, H. K. Kim, R. Rodriguez, K. Keeter, Z. Li, G. Gu, and R. B. James, Journal of Electronic Materials **40**, 274 (2011).

[17]   S. S. Kostina, M. P. Hanson, P. L. Wang, J. A. Peters, D. A. Valverde-Chávez, P. Chen, D. G. Cooke, M. G. Kanatzidis, and B. W. Wessels, ACS Photonics **3**, 1877 (2016).

[18]   J. H. Zhou and S. R. Elliott, Physical Review B **45**, 1668 (1992).

[19]   J. H. Zhou and S. R. Elliott, Physical Review B **46**, 12402 (1992).

[20]   Z. Rivera-Alvarez, L. Hernández, M. Becerril, A. Picos-Vega, O. Zelaya-Angel, R. Ramírez-Bon, and J. R. Vargas-García, Solid State Communications **113**, 621 (2000).

[21]   Y. C. Wu, C. H. Liu, S. Y. Chen, F. Y. Shih, P. H. Ho, C. W. Chen, C. T. Liang, and W. H. Wang, Scientific Reports **5**, 10, 11472 (2015).

[22]   M. C. Tarun, F. A. Selim, and M. D. McCluskey, Physical Review Letters **111**, 5, 187403 (2013).

[23]   J. J. Luo, A. U. Adler, T. O. Mason, D. B. Buchholz, R. P. H. Chang, and M. Grayson, Journal of Applied Physics **113**, 8, 153709 (2013).

[24]   S. Das, J. A. Peters, W. Lin, S. S. Kostina, P. Chen, J.-I. Kim, M. G. Kanatzidis, and B. W. Wessels, The Journal of Physical Chemistry Letters **8**, 1538 (2017).

[25]   D. Redfield and R. H. Bube, *Photoinduced Defects in Semiconductors* (Cambridge University Press, 1996).